DELPHI Collaboration

DELPHI 2001–080 CONF 508
June 3, 2001

Search for single leptoquark production in e^+e^- collisions up to $\sqrt{s}$ =208 GeV with the DELPHI detector

Preliminary

S. Andringa[1], N.Ch. Benekos[2], P. Gonçalves[1], A. Onofre[1], Th.D. Papadopoulou[2], L. Peralta[1], M. Pimenta[1] and B. Tomé[1]

Abstract

A search for single production of scalar and vector leptoquarks of the first generation have been performed using the data collected by the DELPHI detector at LEP. Limits at 95% confidence level on the Yukawa couplings and masses of the leptoquark states were derived from the analysis of the data accumulated in the centre-of-mass energy region of 189 GeV up to 208 GeV with a total integrated luminosity of 539 pb^{-1}.

Contributed Paper for EPS HEP 2001 (Budapest) and LP01 (Rome)

[1] LIP-IST-FCUL, Av. Elias Garcia, 14, 1, P-1000 Lisboa, Portugal
[2] NTUA-National Technical University of Athens, Hellas

1 Introduction

In e^+e^- colliders such as LEP it is possible to search for New Physics in topologies where the expected Standard Model (SM) contributions are low or negligible. Events where all or most particles are grouped in one direction in space (in a monojet-like topology) with one isolated lepton (charged or neutral) are a good example of such processes. This final state could be a signature of leptoquark production.

Leptoquarks are coloured spin 0 or spin 1 particles which carry both baryon and lepton quantum numbers. These particles are predicted by a variety of extensions of the SM, from Grand Unified Theories [1] to Technicolor [2] and composite models [3]. They have electric charges of $\pm 5/3$, $\pm 4/3$, $\pm 2/3$ and $\pm 1/3$, and decay into a lepton-quark pair through the charged decay mode ($L_q \to l^{\pm} q$) and/or the neutral decay mode ($L_q \to \nu q$). The relative importance of the two possible decay modes depends on the leptoquark type and is usually given in terms of the charged branching ratio, β.

Leptoquarks can be pair or singly produced at e^+e^- colliders. Only the single leptoquark search is considered in this analysis.

The existence of leptoquarks is constrained indirectly by low-energy data [4] and precision measurements of the Z^0 widths [5]. Leptoquarks below the TeV mass range and with couplings of the order of the electromagnetic coupling should not couple to diquarks in order to prevent proton decay. They should couple chirally to either left or right handed quarks but not to both, and mainly diagonally, i.e., they should couple to a single leptonic generation and to a single quark generation.

Previous results from DELPHI and the other LEP experiments can be found in [6] and [7].

2 Leptoquark phenomenology

The most general Lagrangian which describes the leptoquark couplings can be written [8]:

$$\mathcal{L} = \mathcal{L}_{F=2} + \mathcal{L}_{F=0}, \tag{1}$$

where

$$\begin{aligned} \mathcal{L}_{F=2} = {} & (g_{1L}\bar{q}_L^c i\tau_2 l_L + g_{1R}\bar{u}_R^c e_R)S_1 + \tilde{g}_{1R}\bar{d}_R^c e_R \tilde{S}_1 \\ & + g_{3L}\bar{q}_L^c i\tau_2 \overrightarrow{\tau} l_L \overrightarrow{S}_3 + (g_{2L}\bar{d}_R^c \gamma^\mu l_L + g_{2R}\bar{q}_L^c \gamma^\mu e_R)V_{2\mu} \\ & + \tilde{g}_{2L}\bar{u}_R^c \gamma^\mu l_L \tilde{V}_{2\mu} + c.c. \end{aligned} \tag{2}$$

and

$$\begin{aligned} \mathcal{L}_{F=0} = {} & (h_{2L}\bar{u}_R l_L + h_{2R}\bar{q}_L i\tau_2 e_R)R_2 + \tilde{h}_{2L}\bar{d}_R l_L \tilde{R}_2 \\ & + (h_{1L}\bar{q}_L \gamma^\mu l_L + h_{1R}\bar{d}_R \gamma^\mu e_R)U_{1\mu} + \tilde{h}_{1R}\bar{u}_R \gamma^\mu e_R \tilde{U}_{1\mu} \\ & + h_{3L}\bar{q}_L \overrightarrow{\tau} \gamma^\mu l_L \overrightarrow{U}_{3\mu} + c.c. \end{aligned} \tag{3}$$

and where q_L, l_L are the left-handed quark and lepton doublets, and e_R, d_R, u_R are the right-handed charged leptons, down and up quarks respectively. The subscript L and R of the coupling constants stand for the lepton chirality and the indices of the leptoquarks give

the dimension of their SU(2) representation. Colour, weak isospin and generation flavour indices have been suppressed. The leptoquarks S (i.e. $S_1, \tilde{S}_1, \overrightarrow{S}_3$) and V (i.e. $V_2, \tilde{V}_2$) have fermion number F=3B+L=-2 (B and L are the baryon and lepton numbers, respectively). The leptoquarks R (i.e. $R_2, \tilde{R}_2$) and U (i.e. $U_1, \tilde{U}_1, \overrightarrow{U}_3$) have fermion number F=3B+L=0. The quantum numbers of different leptoquark types are summarised in table 1 [8]. Every coupling $g_{1L}, ..., h_{3L}$ can be replaced by a generic Yukawa coupling g which can be related to electromagnetic strength by allowing k to vary in $g^2/(4\pi) = k\alpha_{em}$. The effective coupling given in the table for each leptoquark type is generically referred to as λ by some authors. It should be noted that while $\lambda = g$ for most leptoquark types, $\lambda = \sqrt{2}g$ for S_3(-4/3) and U_3(-5/3).

Scalar LQs	Q	decay mode(s)	coupling(s)
S_1	-1/3	$e_L^- u$,νd	g_{1L},$-g_{1L}$
	-1/3	$e_R^- u$	g_{1R}
$\tilde{S}_1$	-4/3	$e_R^- d$	$\tilde{g}_{1R}$
S_3	-4/3	$e_L^- d$	$-\sqrt{2}g_{3L}$
	-1/3	$e_L^- u$,νd	$-g_L$,$-g_L$
R_2	-5/3	$e_L^- \bar{u}$	h_{2L}
	-5/3	$e_R^- \bar{u}$	h_{2R}
Vector LQs	Q	decay mode(s)	coupling(s)
V_2	-4/3	$e_L^- d$	g_{2L}
	-4/3	$e_R^- d$	g_{2R}
	-1/3	$e_R^- u$	g_{2R}
$\tilde{V}_2$	-1/3	$e_L^- u$	$\tilde{g}_{2L}$
U_1	-2/3	$e_L^- \bar{d}$,$\nu \bar{u}$	h_{1L},h_{1L}
	-2/3	$e_R^- \bar{d}$	h_{1R}
$\tilde{U}_1$	-5/3	$e_R^- \bar{u}$	$\tilde{h}_{1R}$
U_3	-5/3	$e_L^- \bar{u}$	$\sqrt{2}h_{3L}$
	-2/3	$e_L^- \bar{d}$,$\nu \bar{u}$	$-h_{3L}$,h_{3L}

Table 1: Characterization of the different scalar and vector leptoquarks considered in this paper. For each leptoquark type the charge, the decay modes and the effective coupling are given.

2.1 Single production in $e^{\pm}\gamma$ and e^+e^- collisions

Single production of leptoquarks in $e\gamma$ collisions was discussed by several authors in the literature, using basically two different frameworks. In the first one, the direct or perturbative approach, the tree-level diagrams shown in figure 1 are directly computed. In the second framework, the resolved photon approach, only the dominant diagram with

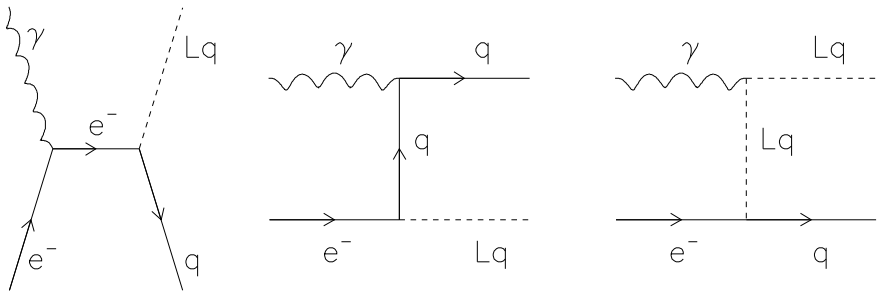

Figure 1: The perturbative approach: Feynmann diagrams contributing to single leptoquark production in $e^{\pm}\gamma$ collisions (Lq stands for S,V,R and U leptoquarks and q represents either a quark or anti-quark).

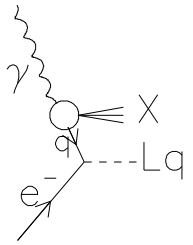

Figure 2: The resolved photon contribution for single leptoquark production in $e\gamma$ collisions (Lq stands for S,V,R and U leptoquarks).

a quark exchanged in the t-channel is considered but the resolved photon contribution is taken into account (see figure 2).

The corresponding diagrams for e^+e^- collisions are shown in figures 3 and 4 for the direct and resolved photon approaches, respectively. They can be interpreted as the previously shown $e\gamma$ diagrams, with the γ emitted by one of the incident electrons. In fact, the computation of the cross-section for single leptoquark production in e^+e^- collisions is usually performed by convoluting the $e\gamma$ process with the energy spectrum of the photon parameterised by the Weizsacker-Williams distribution, $F_{\gamma/e}(x)$ [9].

In [10, 11, 12] the study of leptoquark single production in e^+e^- and $e^{\pm}\gamma$ collisions was carried out using the direct approach. It is worth noting that in [11] the Yukawa coupling constant g associated to the $eqS(V,R,U)$ vertex has a different definition in the Lagrangian compared to that of [10]. Both results are compatible with the replacement $k \to 2k$ in [10].

In [13, 15, 16] the resolved photon approach was used. The interactions initiated by resolved photons are described by the convolution of the photon energy function $F_{\gamma/e}$ with the quark and gluon contents of the photon P_γ (i.e. $\int dx/x F_{\gamma/e}(x) P_\gamma(x)$) [13]. Since the production cross-section is proportional to $(1+q)^2$ (where q is the leptoquark charge), leptoquarks of charge $q = -1/3(-2/3)$ and $q = -5/3(-4/3)$ have similar production

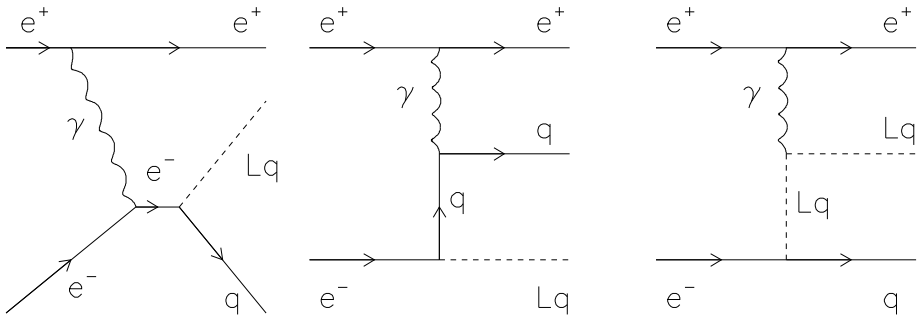

Figure 3: The perturbative approach: Feynmann diagrams for single leptoquark production in e^+e^- collisions (Lq stands for S,V,R and U leptoquarks).

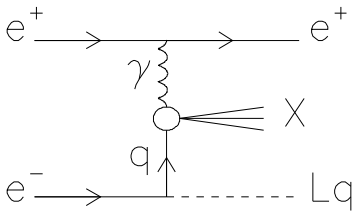

Figure 4: The resolved photon contribution for single leptoquark production in e^+e^- collisions (Lq stands for S,V,R and U leptoquarks).

cross-sections [14]. For the same leptoquark charge, the vector production cross-section is the double of the scalar one. The coupling convention adopted in [15] is different from the one defined by [11]; results with $k = 0.5$ in [15] are equivalent to results in [11] $k = 1$.

As discussed in [15] the non-perturbative contribution taken into account in the resolved photon approach cannot be neglected in $e\gamma$ interactions, where the perturbative processes are $O(\alpha_{em}^2)$ while the hard subprocess in the resolved photon case ($eq \rightarrow S(V, R, U)$) is $O(\alpha_{em})$. The distribution function of partons in the photon is $O(\alpha_{em}/\alpha_s)$ which makes the resolved photon contribution $O(\alpha_{em}^2/\alpha_s)$. There is, in addition to the point like contribution $\gamma \rightarrow q\bar{q}$, a vector meson dominance contribution to the photon structure which increases the resolved photon contribution to the total cross-section even further. However, as it will be shown below, the difference between the two approaches is not very significant in e^+e^- collisions in the mass range explored in this paper.

Both frameworks were considered in this analysis. The PYTHIA generator [17] was used for the resolved photon approach and the ERATO generator [18] was used for the perturbative approach.

2.1.1 Perturbative approach

In this framework the ERATO Monte Carlo (MC) program [18] was used to generate scalar and vector leptoquarks and evaluate the corresponding cross-sections. In ERATO, the generation of a specific leptoquark signal results in a three particle final state (lqq or νqq) taking into account the contributions from the known SM processes and their interferences with the leptoquark diagrams. ERATO has also the possibility of distinguishing different types of scalar and vector leptoquarks by choosing appropriate input parameters.

The decay widths of the leptoquarks are parameterised by:

$$\Gamma_J = f_J \frac{M}{8\pi} \sum_{i=1}^{N_{ch}} g_i^2, \tag{4}$$

where $J = 0, 1$, $f_0 = 1/2$ and $f_1 = 1/3$, and $N_{ch} = 1, 2$ depending on the available channels.

The value of the cross-sections evaluated by ERATO concern only production of negatively charged leptoquarks. To take into account the production of leptoquarks and antileptoquarks, the ERATO cross-sections were multiplied by a factor 2.

2.1.2 Resolved photon approach

In this framework a modified version of the PYTHIA Monte Carlo program was implemented to generate both scalar and vector leptoquarks. The Drees and Grassie parametrisation of the structure function of the photon $P_\gamma(x)$ [19] was used in the generator. The photon energy spectrum $F_{\gamma/e}(x)$ was parameterized according to the Equivalent Photon Approximation [20] and the maximum kinematically allowed squared four-momentum transfer Q^2_{max} was set to $s/4$.

The PYTHIA total production cross-section can be compared to the one from references [14, 15], which uses the Weizsacker-Williams approximation for the photon energy spectrum and the Glück Reya Vogt parameterisation (GRV) [21] for the photon parton distribution. The approach used [14] is independent of the leptoquark chirality (i.e., leptoquarks can couple to either right or left handed particles but not to both) and is almost insensitive to whether the leptoquark is scalar or vector. The cross-section evaluated by PYTHIA describe already the production of leptoquarks and anti-leptoquarks, while in [15] only production of negatively charged leptoquarks is considered.

2.1.3 Cross-section comparisons

The cross-sections for single scalar leptoquark production at centre-of-mass energy $\sqrt{s}$ =208 GeV are shown in figure 5, as a function of the leptoquark mass for different charges. The cross-sections were computed according to references [10] and [14] or given by the two MC programs described above, using a common coupling definition. Taking as a reference the Pakvasa parameterisation [11], k=2 should be considered in [10], while k=0.5 must be taken in [15, 14]. The couplings for PYTHIA and ERATO were also fixed to this definition.

As it can be observed, significant differences exist in the low mass region, where the resolved contribution is important. At high masses a good agreement between the

different models and generators is observed, with differences below 20% in the interesting mass region.

3 Data samples

Data were collected at $\sqrt{s}$ ranging from 189 GeV to 208 GeV and correspond to a total integrated luminosity of 539 pb^{-1}. The luminosity collected at each centre-of-mass energy is given in table 2. A detailed description of the DELPHI detector, its performance, trigger and readout chain can be found in [22].

$\sqrt{s}$ (GeV)	189	192	196	200	202	205	207	208
Luminosity (pb $^{-1}$)	151.7	25.9	76.4	83.5	40.1	77.1	76.6	7.7

Table 2: Luminosity collected by DELPHI for each centre-of-mass energy. For $\sqrt{s} >$ 202 GeV the data were collected during the year 2000 and split into two energy bins.

The background process $e^+e^- \to Z\gamma$ was generated with PYTHIA 6.125. For $\mu^+\mu^-(\gamma)$ and $\tau^+\tau^-(\gamma)$, DYMU3 [23] and KORALZ 4.2 [24] were used, respectively, while the BHWIDE generator [25] was used for Bhabha events. Simulation of four-fermion final states was performed using EXCALIBUR [26] and GRC4F [27]. Two-photon interactions with hadronic final states were generated using TWOGAM [28]. The generated signal and background events were passed through the detailed simulation of the DELPHI detector and then processed with the same reconstruction and analysis programs as the real data.

4 Analyses description

Event topologies characterised by an energetic monojet were searched for. In the charged decay mode a well isolated charged lepton should also be present. After a common preselection level in which monojet-like events were selected, different preselection cuts were used in the charged and neutral decay mode analysis to identify the correct event topology. In both decay modes, discriminant analyses were then used.

4.1 Event preselection

Events with at least seven charged particles (excluding the isolated charged lepton if present), a total visible energy (E_{vis}) larger then $0.2\sqrt{s}$ and no isolated photons were selected.

The reconstruction of isolated leptons consisted on constructing double cones centered in the direction of the charged particles and requiring the energy in the inner (half opening angle of 5°) to be above 4 GeV. The energy contained between the inner and the outer cone was required to be small, to ensure isolation. Both the opening angle of the outer cone and the cut on the energy contained between the two cones were allowed to vary according

$\sqrt{s}$ **(GeV)**	*Leptoquark Charged Decay Data (SM)*	*Leptoquark Neutral Decay Data (SM)*
189	147 (179.0±5.2)	432 (429.2±10.4)
192	27 (31.0±0.9)	79 (82.4±1.9)
196	96 (93.0±2.7)	275 (231.5±5.6)
200	97 (108.0±3.1)	279 (253.8±5.9)
202	53 (52.0±1.5)	137 (122.1±2.9)
205	114 (97.0±3.1)	243 (223.2±4.8)
207	92 (93.0±2.8)	228 (219.7±5.5)
208	6 (8.0±0.3)	18 (19.7±0.6)
TOTAL	632 (661.0±8.0)	1691 (1581.6±15.5)

Table 3: Number of data events and expected SM contributions for the charged and neutral decay modes at the preselection level for the different centre-of-mass energies.

to the energy and classification of the reconstructed particle. Lepton identification was based on the standard DELPHI algorithms described in [22, 29].

The Durham jet algorithm [30] was used to force all particles in the event except isolated leptons into one and two jets. While the monojet topology characterises the signal, the two jet configuration was used in background rejection. The momentum of the monojet was required to be larger than 10 GeV/c, and its polar angle to be between 20° and 160°. In the forced monojet configuration, background from multijet events was reduced by rejecting events with more than 20 tracks in the hemisphere opposite to the direction of the monojet. Contamination from Bhabha events was reduced by requiring the ratio E_{em}/p for the monojet to be lower than 0.95.

Specific selection criteria were then applied in the charged and neutral decay mode analyses and are described below. Table 3 shows, at the end of the preselection, the number of events in data, together with the expected SM background for the different centre-of-mass energies.

4.1.1 Charged decay mode

In the charged decay mode ($Lq \rightarrow e^{\pm}q$) a well isolated electron is expected in the event. Therefore, events were selected if an identified electron with a momemtum above 10 GeV/c, a polar angle between 20° and 160° and isolated by more than 20° was found. Isolated leptons were loosely identified as electrons if they had no associated hits in the muon chambers, an electromagnetic energy (E_{em}) greater than $0.5\mathrm{E}_{vis}$ and a ratio E_{em}/p_{ℓ}, where p_{ℓ} is the lepton momentum, larger than 0.2.

In this topology, contamination from Bhabha and 2-photon interaction events was further reduced by requiring the polar angle of the missing momentum to be above 15° and below 165° and the monojet-lepton invariant mass to be greater than 50 GeV/c^2.

In addition, the multiplicity in the hemisphere opposite to the monojet direction was required to be below 10.

Figures 6 and 7 show distributions of relevant variables at the preselection level, together with the SM expectation for a centre-of-mass energy of 207 GeV. A good agreement is observed.

4.1.2 Neutral decay mode

In the neutral decay mode ($Lq \to \nu q$) analysis no isolated leptons were allowed in the final state. In this channel the monojet polar angle was required to be between 30° and 150°, and $-log_{10}(y(2 \to 1))$, where $y(2 \to 1)$ is the Durham resolution variable in the transition from two jets to one jet, was required to be greater than 0.3.

Figure 8 shows distributions of relevant variables at the preselection level, together with the SM expectation for a centre-of-mass energy of 207 GeV. A good agreement is observed.

4.2 Discriminant analysis

For the preselected events a signal likelihood ($\mathcal{L}_S$) and a background likelihood ($\mathcal{L}_B$) were constructed using probability density functions based on relevant kinematic variables. The discriminating variable was defined according to $\mathcal{L}_S/\mathcal{L}_B$. For both the charged and the neutral decay mode analysis, the signal and background likelihood distributions were constructed by using the following variables:

- the momentum of the monojet;
- $-log_{10}(y(2 \to 1))$;

and, clustering the events into two jets:

- the invariant mass of the two jets;
- the momentum of the less energetic jet;
- the angle between the two jets.

In the charged decay mode analysis, two additional variables involving the isolated lepton were used:

- the lepton momentum;
- the monojet-lepton acoplanarity.

Events with signal likelihood probability $log_{10}(\mathcal{L}_S)$ greater than -1.95 (-2.0) and likelihood ratio $log_{10}(\mathcal{L}_S/\mathcal{L}_B)$ greater than -2.0 (2.0) were kept in the charged (neutral) decay mode analysis. In figure 9 likelihood ratio distributions are shown.

5 Results and limits

Single production of first generation leptoquarks was searched for in both the charged and neutral decay modes. The results of the analysis are presented and discussed below.

$\sqrt{s}$ **(GeV)**	*Leptoquark Charged Decay Data (SM)*	*Leptoquark Neutral Decay Data (SM)*
189	15 (15.2±1.9)	6 (7.7±1.1)
192	2 (2.5±0.3)	3 (1.5±0.2)
196	8 (7.4±0.9)	4 (4.2±0.6)
200	6 (9.3±1.2)	8 (4.4±0.6)
202	6 (4.5±0.6)	4 (2.1±0.3)
205	8 (6.5±1.2)	5 (4.6±0.5)
207	8 (7.9±1.3)	4 (4.8±0.6)
208	0 (0.8±0.1)	0 (0.4±0.1)
TOTAL	53 (54.1±3.1)	34 (29.7±1.6)

Table 4: Number of data events and expected SM contributions for the charged and neutral decay modes after the likelihood ratio cut for the different centre-of mass-energies.

5.1 Selected events

In table 4 the number of events selected in the charged and neutral decay mode analyses are shown, together with the expected SM background for the different centre-of-mass energies. A good agreement between observation and expectation is found.

Figure 10 shows the reconstructed mass distributions of selected candidates, together with the SM background, for both the charged and neutral decay mode analysis.

5.2 Signal efficiencies and cross-sections

As discussed above, single leptoquark production signals were studied considering both the direct and resolved frameworks. For the direct framework, the ERATO generator was used for signal generation and cross-section evaluation. For the resolved framework, signal efficiencies were computed using the modified version of PYTHIA described in section 2.1.2. The total cross-sections were estimated using reference [15]. In both cases the couplings were scaled down to $g = \sqrt{4\pi\alpha_{em}}$.

Selection efficiencies and mass resolutions were extracted as a function of the leptoquark mass. The signal mass resolution varies from 25 GeV/c^2 to 35 GeV/c^2 for masses between 140 GeV/c^2 and 200 GeV/c^2. The signal efficiencies obtained with the PYTHIA and ERATO generators for scalar and vector leptoquarks are shown in tables 5 and 6 for the charged and neutral decay mode analysis, respectively.

5.3 Leptoquark mass and coupling limits

Limits were derived using the modified frequentist likelihood ratio method [32]. For the leptoquark types with $\beta = 0.5$ the charged and neutral decay mode analyses were combined.

Charged Decay Mode	$\sqrt{s} = 200$ **GeV** ($m = 140 \rightarrow 200$ GeV/c^2)	$\sqrt{s} = 206$ **GeV** ($m = 140 \rightarrow 200$ GeV/c^2)
$\epsilon_{scalar\ PYTHIA}$	$21.4 \pm 2.1\% \rightarrow 55.8 \pm 3.3\%$	$23.5 \pm 1.5\% \rightarrow 52.6 \pm 2.3\%$
$\epsilon_{scalar\ ERATO}$	$26.1 \pm 2.5\% \rightarrow 53.0 \pm 3.3\%$	$22.3 \pm 1.5\% \rightarrow 50.2 \pm 2.2\%$
$\epsilon_{vector\ PYTHIA}$	$21.0 \pm 2.1\% \rightarrow 52.6 \pm 3.2\%$	$19.9 \pm 1.4\% \rightarrow 49.1 \pm 2.2\%$
$\epsilon_{vector\ ERATO}$	$28.0 \pm 2.4\% \rightarrow 41.7 \pm 2.9\%$	$20.8 \pm 1.4\% \rightarrow 41.8 \pm 2.1\%$

Table 5: Signal efficiency for the charged decay mode at the final selection level for the different generators, masses and centre-of-mass energies.

Neutral Decay Mode	$\sqrt{s} = 200$ **GeV** ($m = 140 \rightarrow 200$ GeV/c^2)	$\sqrt{s} = 206$ **GeV** ($m = 140 \rightarrow 200$ GeV/c^2)
$\epsilon_{scalar\ PYTHIA}$	$44.0 \pm 2.9\% \rightarrow 64.3 \pm 4.0\%$	$42.5 \pm 2.1\% \rightarrow 62.1 \pm 2.5\%$
$\epsilon_{scalar\ ERATO}$	$41.8 \pm 2.9\% \rightarrow 67.2 \pm 3.7\%$	$42.2 \pm 2.1\% \rightarrow 62.5 \pm 2.1\%$
$\epsilon_{vector\ PYTHIA}$	$44.0 \pm 2.9\% \rightarrow 64.3 \pm 4.0\%$	$42.5 \pm 2.1\% \rightarrow 59.0 \pm 2.1\%$
$\epsilon_{vector\ ERATO}$	$44.8 \pm 2.9\% \rightarrow 56.6 \pm 3.4\%$	$45.1 \pm 2.1\% \rightarrow 52.1 \pm 2.3\%$

Table 6: Signal efficiency for the neutral decay mode at the final selection level for the different generators, masses and centre-of-mass energies.

Using the invariant mass distributions, 95% confidence level (CL) limits on the leptoquark coupling parameter g as a function of its mass were derived in both frameworks, for scalar and vector leptoquarks of different types, and for the different charged decay branching ratios ($\beta = 1$ or $\beta = 0.5$). They are shown in figures 11 and 12, for the direct and resolved photon approach respectively.

Lower limits at 95% CL on the mass of a first generation leptoquark were derived setting the coupling constant $g = \sqrt{4\pi\alpha_{em}}$. The results obtained using the direct framework are given in table 7 for the different leptoquark types and branching ratios. The mass limits obtained within the resolved framework are comparable within 2 GeV/c^2.

Previous limits on the existence of leptoquarks have been set by low energy data [4] and by direct searches at high energies [33, 34, 6, 7]. At the Tevatron the mass of scalar leptoquarks decaying to electron jet pairs was constrained to be above 225 GeV/c^2(213 GeV/c^2) by the D0 (CDF) experiment. The combined limit from the two experiments is 242 GeV/c^2 for a scalar leptoquark. The limits on vector leptoquarks at the TEVATRON are model dependent but are expected to be higher than the ones obtained for scalar leptoquarks. Searches for second and third generation leptoquarks were also performed at the TEVATRON. At HERA limits on the ratio M/λ and on masses of first generation leptoquarks in the range $150 - 280$ GeV/c^2 were set. Searches for Lepton-Flavour-Violation leptoquarks were also performed.

Rare processes, which are forbidden in the SM, also provide strong bounds on the λ/m_{LQ} ratio [35], where λ is the leptoquark-fermion Yukawa type coupling and m_{LQ} is

Scalar LQs	Q	β	*Mass Limit* (GeV/c^2)
S_1	-1/3	0.5	182.
	-1/3	1	183.
$\tilde{S}_1$	-4/3	1	155.
S_3	-4/3	1	173.
	-1/3	0.5	182.
R_2	-5/3	1	184.
	-5/3	1	184.
Vector LQs	Q	β	*Mass Limit* (GeV/c^2)
V_2	-4/3	1	171.
	-4/3	1	171.
	-1/3	1	189.
$\tilde{V}_2$	-1/3	1	189.
U_1	-2/3	0.5	169.
	-2/3	1	170.
$\tilde{U}_1$	-5/3	1	189.
U_3	-5/3	1	196.
	-2/3	0.5	169.

Table 7: Lower limits (in GeV/c^2) at 95% confidence level on the mass of first generation leptoquarks for $g = \sqrt{4\pi\alpha}$.

the leptoquark mass.

6 Summary

A search for first generation leptoquarks was performed using data collected by the DELPHI detector at centre-of-mass energies in the range between 189 GeV and 208 GeV for an integrated luminosity of 539 pb^{-1}. Both neutral and charged decay modes of scalar and vector leptoquarks were searched for. Two different phenomenological approaches were considered. No evidence for a signal was found in the data. Limits on leptoquark masses and couplings were set at 95% confidence level.

Acknowledgements

We would like to thank M. Doncheski and C. Papadopoulos for the very useful discussions on the leptoquark production. We are greatly indebted to our technical collaborators and to the funding agencies for their support in building and operating the DELPHI detector. We are grateful to Jonh Guy for his collaboration. The NTUA group would

like to acknowledge the support of the program for Basic Research "Archimidis" of ICCS-NTUA. Very special thanks are due to the members of the CERN-SL Division for the excellent performance of the LEP collider.

References

[1] P. Langacker, Phys. Rep. **72** (1981) 185.

[2] See for example S. Dimopoulos, Nucl. Phys. **B168** (1981) 69.

[3] See for example B. Schremp and F. Schremp, Phys. Lett. **153B** (1985) 101.

[4] O. Shanker, Nucl. Phys. **B204** (1982) 375; W. Buchmuller and D.Wyler, Phys. Lett. **B177** (1986) 377; J.L. Hewett and T.G. Rizzo, Phys. Rev. **D36** (1987) 3367; M. Leurer, Phys. Rev. **D49** (1994) 333 and Phys. Rev. **D50** (1994) 536.

[5] J.K. Mizukoshi, O.J.P. Eboli and M.C. Gonzalez-Garcia, CERN-TH 7508/94 (1994); G. Bhattacharya, J. Ellis and K. Sridhar, CERN-TH 7280/94 (1994).

[6] DELPHI Coll., P. Abreu et al., Phys.Lett. **B446** (1999) 62. DELPHI Coll., P. Abreu et al., Phys. Lett. **B316** (1993) 620;

[7] ALEPH Coll., D. Decamp et al., CERN PPE/91-149. ALEPH Coll., M. N. Minard et al., CERN-OPEN-99-338; L3 Coll., B. Adeva et al., Phys. Lett. **B261** (1991) 169; L3 Coll., M. Acciarri et al., CERN-EP-2000-061; OPAL Coll., G. Alexander et al., Phys. Lett. **B263** (1991) 123; OPAL Coll., G. Abbiendi et al., CERN-EP-2001-040, subm. Eur. Phys.;

[8] W. Buchmuller, R.Ruckl, D.Wyler, Phys. Lett. **B191** (1987) 442;

[9] C.F.von Weizsacker, Z.Phys. **88** (1934) 612; E.J.Williams, Phys. Rev. **45** (1934) 729; M.Chen, P.Zerwas, Phys.Rev.**D12** (1975) 187.

[10] H.Nadeau, D.London, Phys. Rev D **47** (1993) 3742.

[11] J.L.Hewett, S.Pakvasa, Phys. Lett. **B227** (1989) 178.

[12] H.Nadeau, D.London, G.Bélanger, UdeM-LPN-TH-93-160, McGill-93/29, hep-ph/9309243, September 1993.

[13] O.J.P.Eboli, E.M.Gregores, M.B.Magro, P.G.Mercadante, S.F.Novaes, Phys. Lett. **B311** (1993) 147-152.

[14] M. Doncheski and S. Godfrey, Phys. Lett. **B393** (1997) 355.

[15] M. Doncheski and S. Godfrey, Phys. Rev. **D49** (1994) 6220.

[16] A.Djouadi, J.Ng, T.G.Rizzo, SLAC-PUB-95-6772, GPP-UdeM-TH-95-17, TRI-PP-95-05, June 1995.

[17] T. Sjöstrand, Comp. Phys. Comm. **82** (1994) 74;
T. Sjöstrand, Pythia 5.7 and Jetset 7.4, CERN-TH/7112-93.

[18] C.G.Papadopoulos, DEMO-HEP-97/04, hep-ph/9703372, March 1997.

[19] M.Drees, K.Grassie, Z.Phys.**C28** (1985) 451-462.

[20] P.Aurenche, G.A.Schuller (conveners), $\gamma\gamma$ Physics, in "Physics at LEP2", CERN 96-01, eds G.Altarelli, T.Sjostrand and F.Zwirner, Vol.1 (1996) 291.

[21] M. Gluck et al., Phys. Rev. **D46** (1992) 1973 and Phys. Rev. **D45** (1992) 3986.

[22] DELPHI coll., P. Aarnio et al., NIM **A303** (1991) 233;
DELPHI Coll., P. Abreu et al., Nucl. Instr. Methods **A378** (1996) 57.

[23] J.E. Campagne and R. Zitoun, Z. Phys. **C43** (1989) 469.

[24] S. Jadach, B.F.L. Ward and Z. Was, Comp. Phys. Comm. **79** (1994) 503.

[25] S. Jadach, W. Placzek and B.F.L. Ward, Phys. Lett. **B390** (1997) 298.

[26] F.A. Berends, R. Pittau, R. Kleiss, Comp. Phys. Comm. **85** (1995) 437.

[27] J.Fujimoto et al., Comp. Phys. Comm. **100** (1997) 128.

[28] S. Nova, A. Olchevski and T. Todorov, "TWOGAM, a Monte Carlo event generator for two photon physics", DELPHI Note 90-35 PROG 152.

[29] F.Cossutti et al., "REMCLU : a package for the Reconstruction of Electromagnetic CLUsters at LEP200", DELPHI Note 2000-164 PROG 242.

[30] S. Catani et al., Phys. Lett. **B269** (1991) 432.

[31] DELPHI Coll., P. Abreu et al., Phys. Lett. **B393** (1997) 245.

[32] A.L. Read, "Optimal statistical analysis of search results based on the likelihood ratio and its application to the search for the MSM Higgs boson at $\sqrt{s}$=161 and 172 GeV", DELPHI 97-158 PHYS 737.

[33] CDF Coll. and D0 Coll., FERMILAB PUB-98/312-E; CDF Coll., F. Abe et al., Phys. Lett. **79** (1997) 4327; CDF Coll., F. Abe et al., Phys. Lett. **82** (1999) 3206; CDF Coll., T. Affolder et al., Phys. Lett. **85** (2000) 2056; D0 Coll., B. Abbott et al., Phys. Rev Lett. **80** (1997) 4327; D0 Coll., V. M. Abazov et al., Fermilab-Pub-01/057-E, hep-ex/0105072 (2001); D0 Coll., S. Abachi et al., Phys. Rev Lett. **75** (1995) 3618; D0 Coll., B. Abbott et al., Phys. Rev Lett. **81** (1998) 38; D0 Coll., B. Abbott et al., Phys. Rev Lett. **83** (1999) 2896; D0 Coll., B. Abbott et al., Phys. Rev Lett. **84** (2000) 2088;

[34] ZEUS Coll., Breitweg et al., Eur. Phys. J. **C16**, (2000) 253-267; ZEUS Coll., Breitweg et al., Phys. Rev. **D63** (2001) 052002 1-15; ZEUS Coll., M. Derrick et al., Phys. Lett. **B306**, (1993) 173; H1 Coll., 30^{th} International Conference on High-Energy Physics ICHEP2000 (2000) Abstract: 951,952,953, Osaka, Japan, H1prelim-00-062, H1prelim-00-061, H1prelim-00-161; H1 Coll., Adloff C., Eur. Phys. J. **C11** (1999) 447-471; H1 Coll., I. Abt et al., Nucl. Phys. **396**, (1993) 3.

[35] S. Davidson et al., Z. Phys. **C61** (1994) 613.

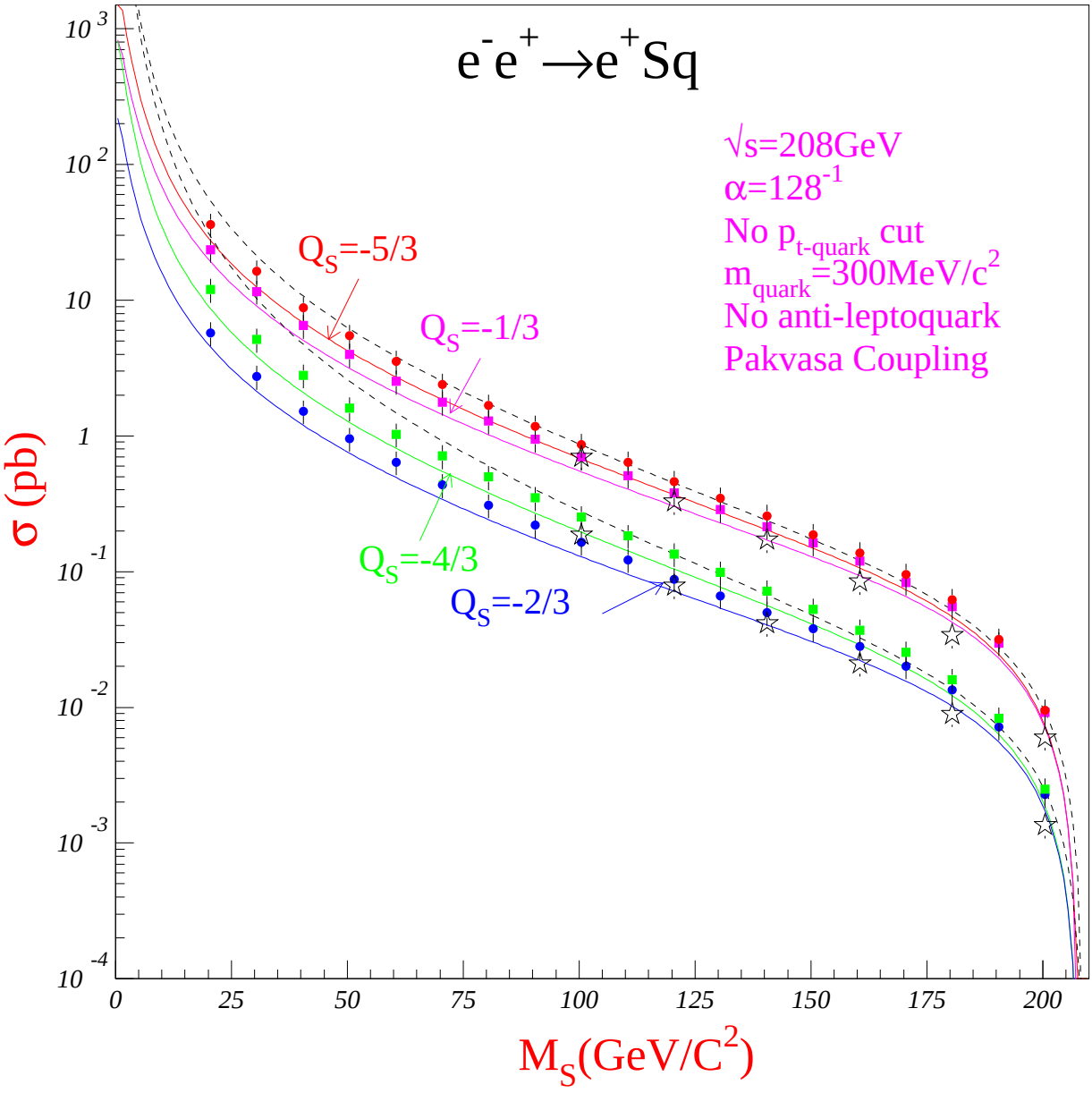

Figure 5: Single scalar leptoquark production cross-section at $\sqrt{s}$ =208 GeV in e^+e^- collisions. The full lines show (for the different leptoquark charges) the cross-section for the perturbative approach (calculated with [10, 12]). The dashed lines show the cross-section for the resolved photon approach [15]. The full points show the ERATO cross-section and the open stars the PYTHIA cross-section.

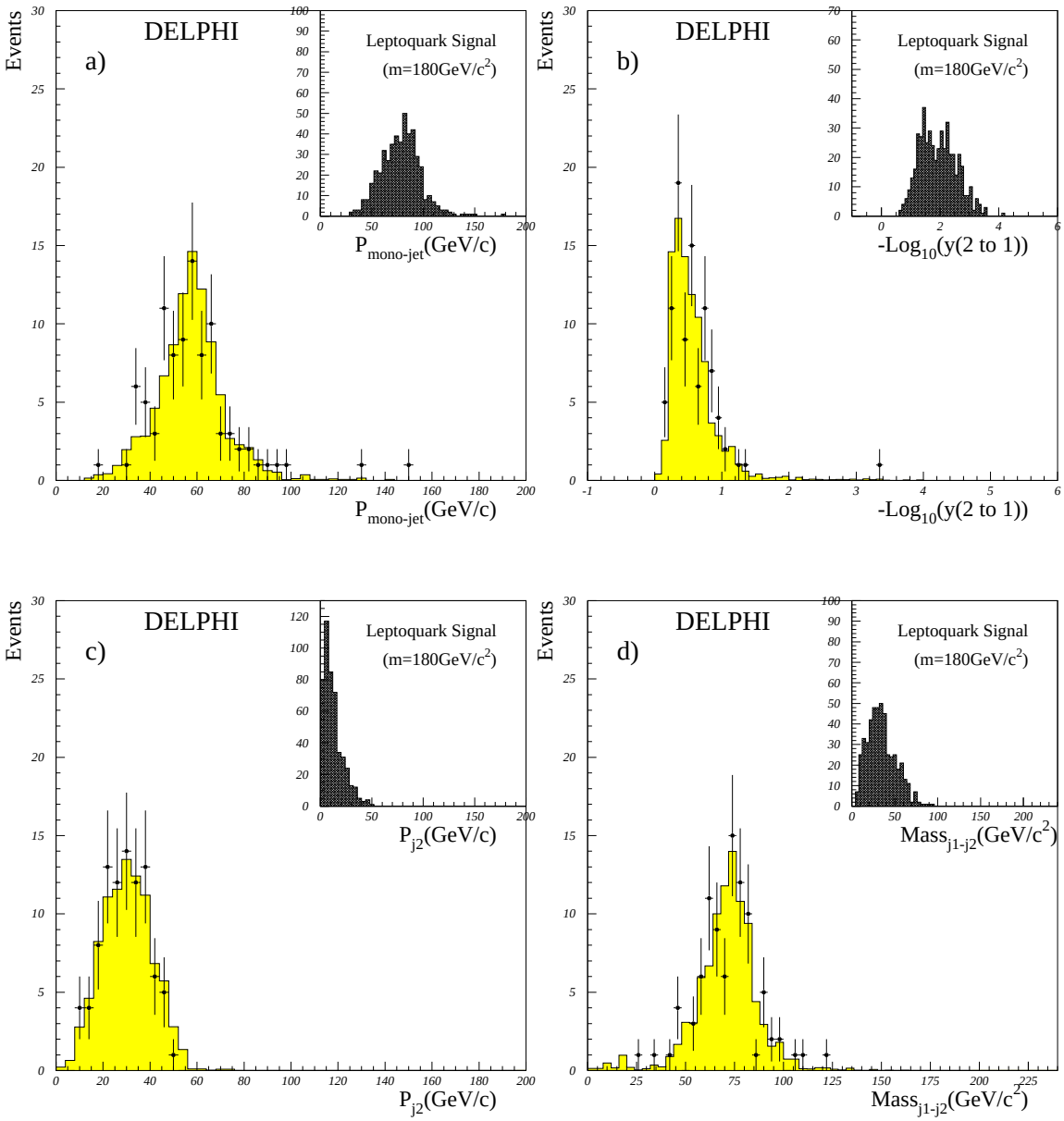

Figure 6: Preselection level of the charged decay mode analysis. The monojet momentum (a), the Durham resolution variable $-log_{10}(y(2 \to 1))$ (b) and, considering the clustering into two jets, the momentum of the less energetic jet (c) and the invariant mass of the two jets (d) are shown. Data at $\sqrt{s}$ =207 GeV (dots) are compared to the background expectations (shaded histogram), while the top right distributions show a leptoquark signal.

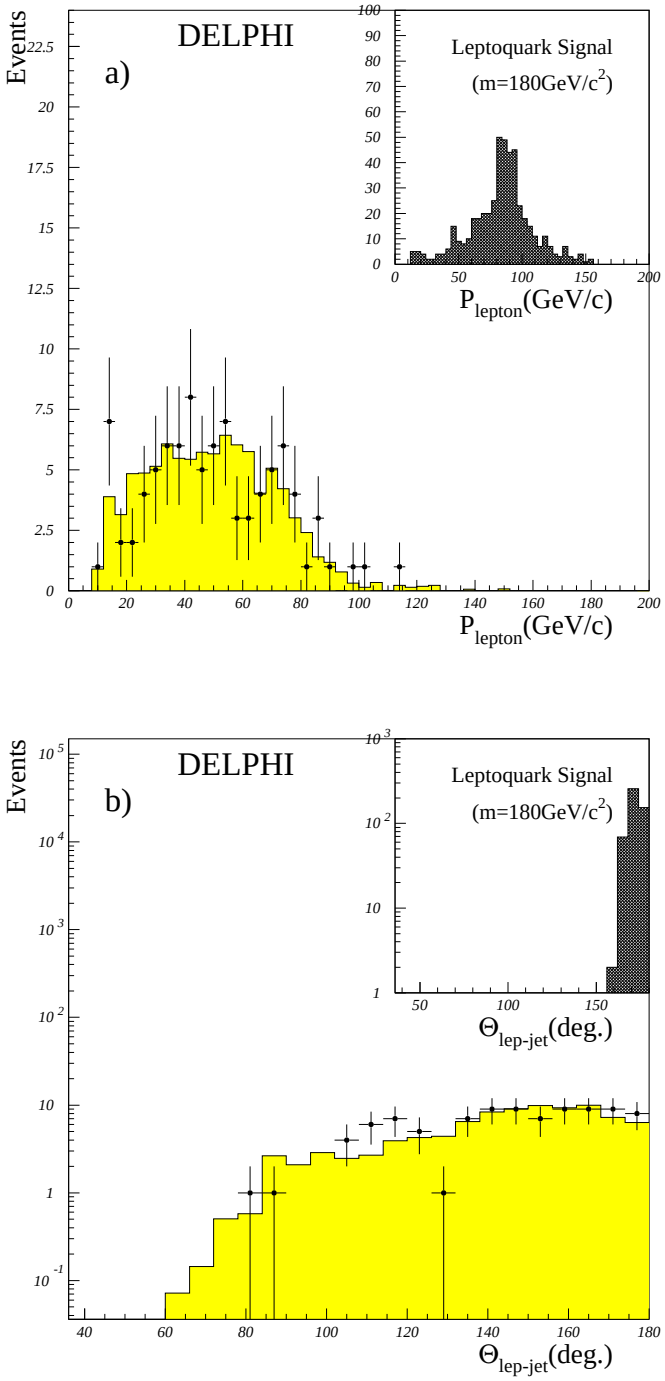

Figure 7: Preselection level of the charged decay mode analysis. The lepton momentum (a) and the angle between the lepton and the monojet (b) are show. The data at $\sqrt{s}$ =207 GeV (dots) are compared to the background expectations (shaded histogram), while the top right distributions show a leptoquark signal.

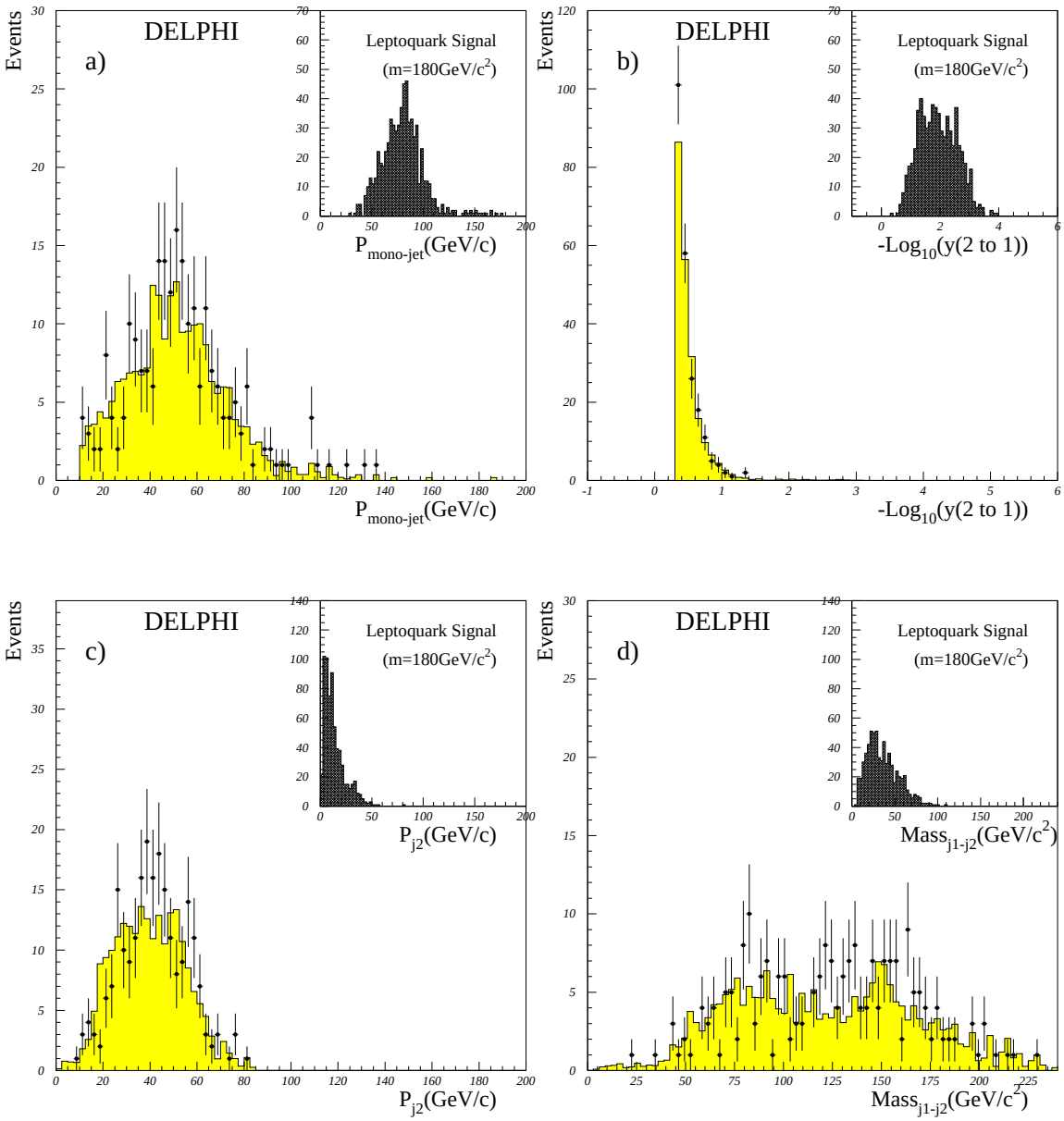

Figure 8: Preselection level of the neutral decay mode analysis. The monojet momentum (a), the Durham resolution variable $-log_{10}(y(2 \to 1))$ (b) and, considering the clustering into two jets, the momentum of the less energetic jet (c) and the invariant mass of the two jets (d) are shown. Data at $\sqrt{s}$ =207 GeV (dots) are compared to the background expectations (shaded histogram), while the top right distributions show a leptoquark signal.

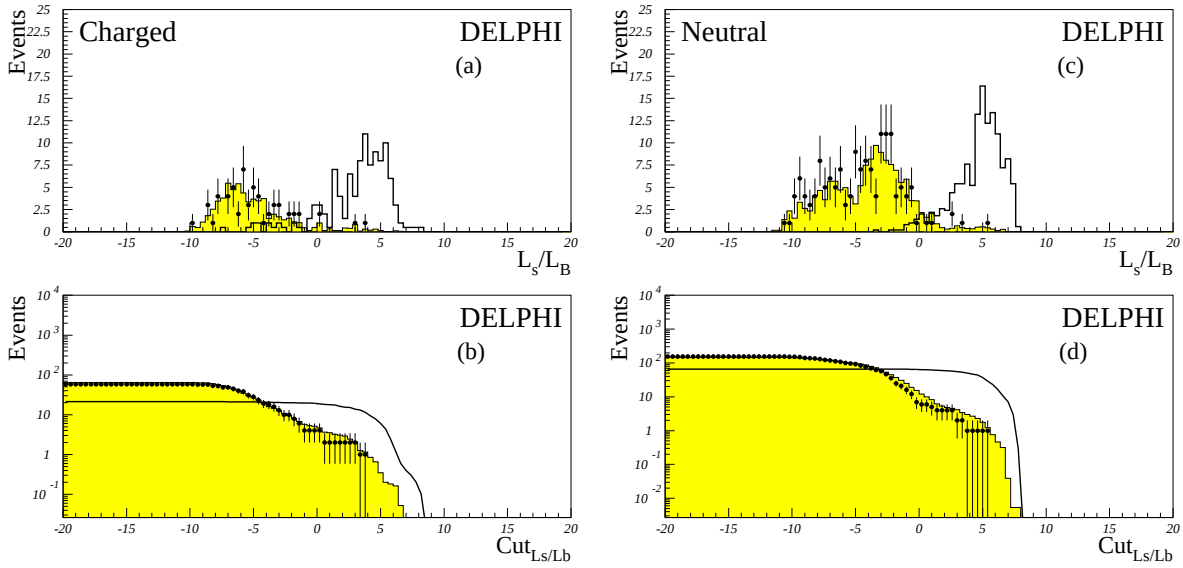

Figure 9: The discriminant variable distributions at the pre-selection level are shown in plots a) and c) for charged and neutral leptoquarks respectively. The bottom plots b) and d) show the corresponding number of events as a function of the cut on the discriminant variable. The data taken at $\sqrt{s}$ =207 GeV (dots) is compared with the expected background (shaded histogram). A leptoquark signal is also shown (the thick line).

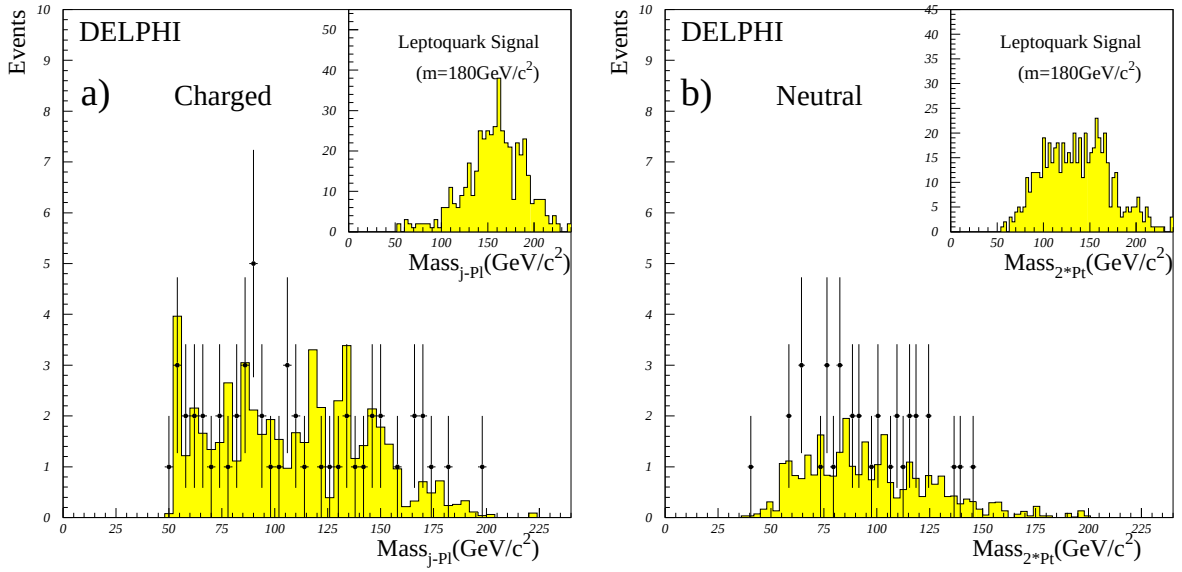

Figure 10: Reconstructed leptoquark mass in charged (a) and neutral (b) decay modes for the selected events at all $\sqrt{s}$. Data (dots) are compared with background expectations (shaded histograms), while the top right distributions show signal distributions for a leptoquark with a mass of 180 GeV/c^2.

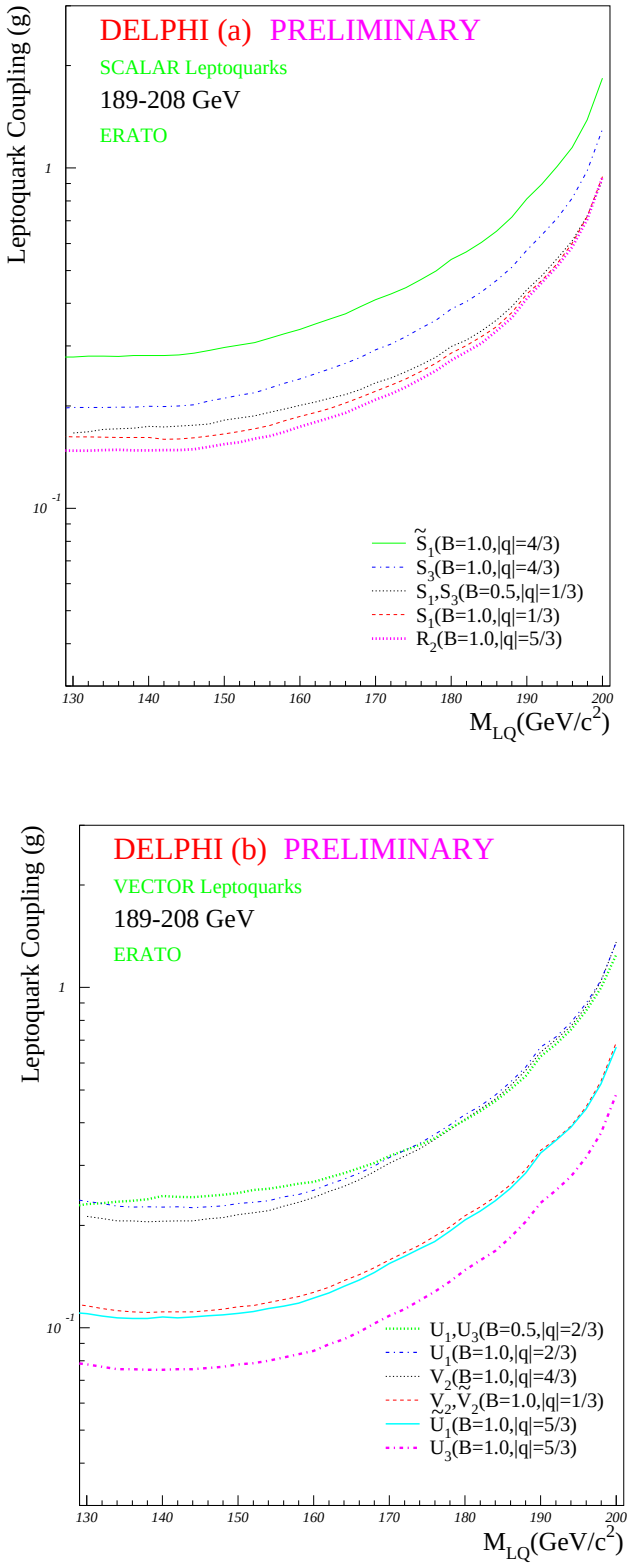

Figure 11: Upper limits on the coupling parameter g of the scalar (a) and vector (b) leptoquarks as a function of the leptoquark mass, in the perturbative approach. The different line types represent the limits obtained for each different leptoquark type.

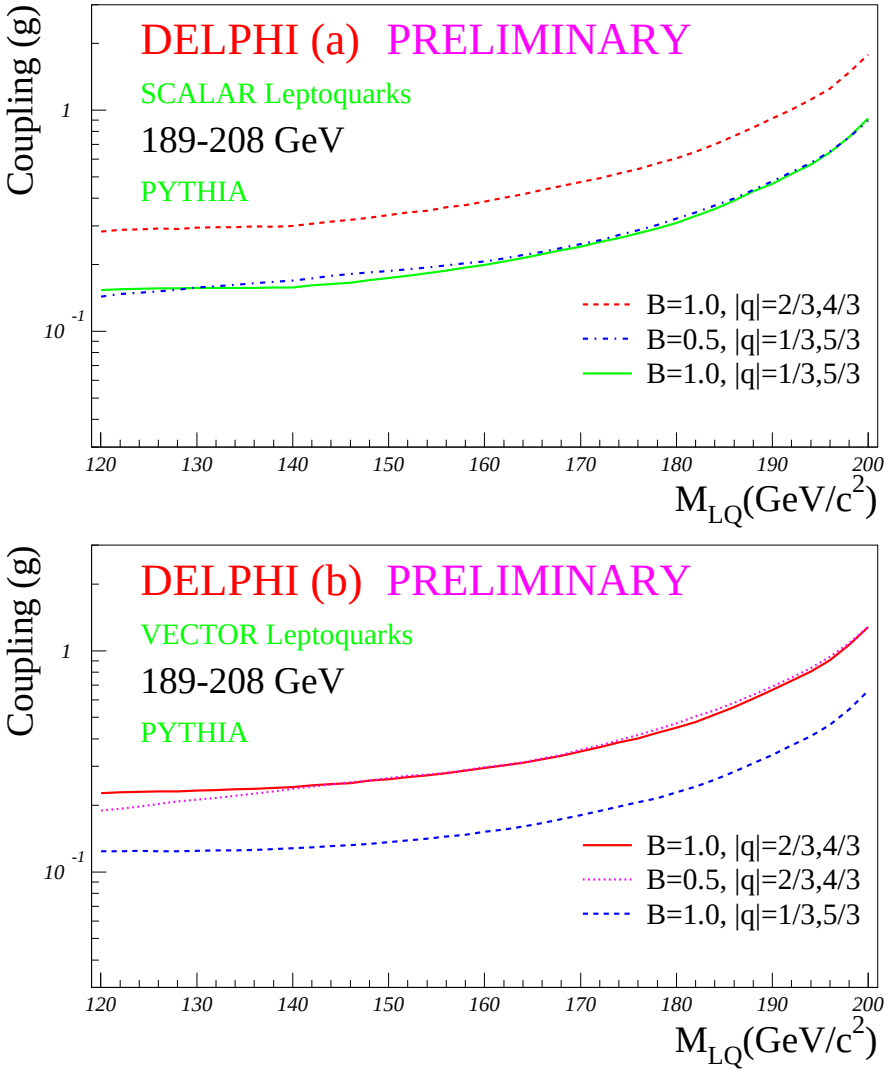

Figure 12: Upper limits on the coupling parameter g of the scalar (a) and vector (b) leptoquarks as a function of the leptoquark mass, in the resolved photon approach. The different line types represent the limits obtained for each different leptoquark type.